EARTHQUAKE ENGINEERING AND STRUCTURAL DYNAMICS
Earthquake Engng Struct. Dyn. —-; **00**:1–17
Published online in Wiley InterScience (www.interscience.wiley.com). DOI: 10.1002/eqe

Dynamic response of out-of-plane loaded one-way spanning URM walls connected to flexible diaphragms

H. Derakhshan*[1], M. C. Griffith[1], and J. M. Ingham[2]

[1]*School of Civil, Environmental, and Mining Engineering, The University of Adelaide, SA 5005, Australia*
[2]*Department of Civil and Environmental Engineering, The University of Auckland, Auckland 1010, New Zealand*

SUMMARY

A simplified numerical model was used to investigate the out-of-plane seismic behaviour of unreinforced masonry (URM) walls. The URM walls were assumed to span vertically between two flexible diaphragms and to have developed a horizontal crack above the wall mid-height. Three degrees of freedom were used to accommodate the wall displacement at the crack height and at the diaphragm connections, and the wall dynamic stability when subjected to different ground motion records was studied. The equations of dynamic motion were obtained using principles of rocking mechanics of rigid bodies and the formulae were next modified to include semi-rigid wall behaviour. A parametric study was conducted that included calculation of the wall response for different values of diaphragm stiffness, wall properties, and earthquake ground motions. The results of the study suggest that stiffening the horizontal diaphragms of typical low-rise URM buildings will amplify the acceleration demand imposed on the wall and especially on the wall-diaphragm connections. This retrofit measure is very likely to improve wall stability but there are certain combinations of wall, diaphragm, and ground motion record characteristics that result in reduced stability for walls connected to stiffened timber diaphragms. It was found that higher storey walls connected to two horizontal diaphragms had reduced stability for applied earthquake accelerograms having dominant frequency content that was comparable to the frequency of the diaphragms. It was also found that there was no clear relationship between wall stability and wall slenderness ratio, which is a relationship that is commonly assumed in the evaluation of the out-of-plane dynamic stability of URM walls. Based on these findings, further study aiming at the development of seismic assessment guidelines for out-of-plane loaded URM walls was suggested. Copyright © —- John Wiley & Sons, Ltd.

Received . . .

KEY WORDS: Brick masonry; Walls; Seismic response; Flexible diaphragm; Stiffness; Out-of-plane

1. INTRODUCTION

Out-of-plane loaded vertically spanning URM walls remain stable for small out-of-plane displacements following wall cracking [1, 2, 3, 4, 5, 6, 7], and a study of this stability is necessary when conducting an effective wall seismic assessment [8]. Support flexibility influences the seismic demand imposed on the out-of-plane loaded walls [1, 9, 10], but most published research works address wall response assuming rigid supports [3, 4, 5, 11, 12].

Several case studies [10, 13, 14] have suggested that higher mode effects due to the relatively long period of flexible diaphragms in URM buildings are detrimental to the seismic stability of out-of-plane loaded walls. It is therefore commonly considered beneficial to strengthen and stiffen existing timber diaphragms to improve expected earthquake response. Conversely, shake table test observations [9] have suggested that for some particular test conditions, walls connected to less stiff

*Correspondence to: Hossein Derakhshan, School of Civil, Environmental, and Mining Engineering, The University of Adelaide, SA 5005, Australia, E-mail: hossein.derakhshan@adelaide.edu.au

diaphragms were more stable than walls connected to stiffer diaphragms, perhaps akin to a base isolation effect.

The purpose of the study reported herein was to investigate the dynamic stability of URM walls including the effects of diaphragm flexibility. Diaphragm flexibility is shown to result in the wall exhibiting several rocking patterns in addition to those relevant for the case of walls connected to rigid supports. It is further shown that walls connected to flexible diaphragms are associated with a reduced out-of-plane rotation capacity when compared to the case of walls connected to rigid diaphragms. To evaluate the wall stability, formula are derived to calculate the wall capacity, a procedure is proposed to calculate the wall displacement demand, and examples of wall stability assessment are provided. The displacement demand imposed on the wall is calculated by considering the post-cracking semi-rigid motion of wall segments utilising an improved wall behavioural model [15] calibrated by laboratory [16] and in-situ [17] tests.

2. WALL MODEL

Fig. 1a shows a rigid block model of an URM wall, and Figs. 1b to 1e show the deformed wall shapes. The translational springs represent the in-plane stiffness of the horizontal diaphragms, and three degrees of freedom (DOF) accommodate the translation and rotation of the wall segments (θ_1, θ_2, and u_b in Fig. 1b to 1e).

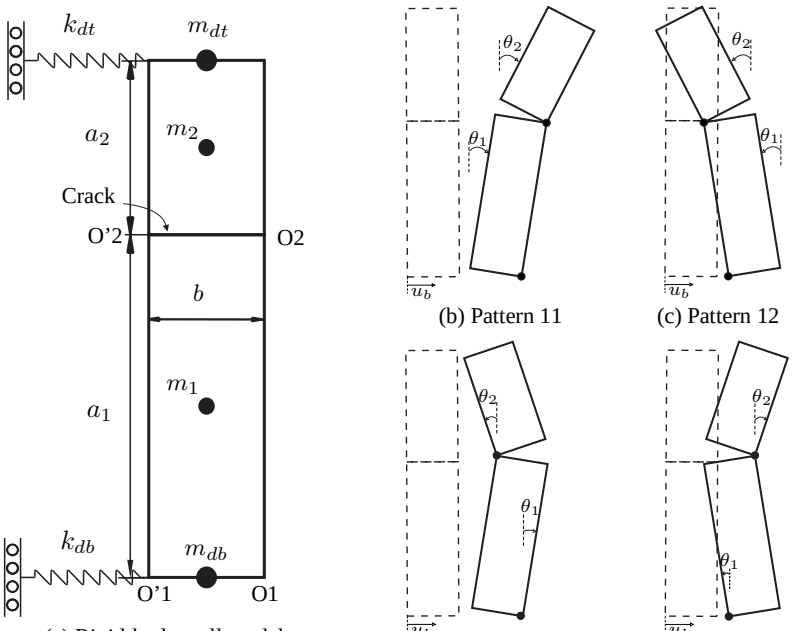

(a) Rigid-body wall model

(b) Pattern 11

(c) Pattern 12

(d) Pattern 21

(e) Pattern 22

Figure 1. Rigid-body wall model

The governing equation of dynamic motion for each pattern shown in Fig 1 is derived using Lagrange's method, and the equations can be shown in the following simple forms:

Patterns 11 and 12:

DOI: 10.1002/eqe

$$\begin{bmatrix} I_{o1}+(m_2+m_{dt})a_1^2 & a_1a_2(\frac{1}{2}m_2+m_{dt}) & m_1a_1+m_{dt}a_1 \\ a_1a_2(\frac{1}{2}m_2+m_{dt}) & I_{o2}+m_{dt}r_d^2 & \frac{1}{2}m_2a_2+m_{dt}a_2 \\ m_1a_1+m_{dt}a_1 & \frac{1}{2}m_2a_2+m_{dt}a_2 & m_1+m_2+m_{db}+m_{dt} \end{bmatrix} \begin{Bmatrix} \ddot{\theta}_1 \\ \ddot{\theta}_2 \\ \ddot{u}_b \end{Bmatrix}$$

$$+ \begin{bmatrix} -(\frac{1}{2}m_1+m_2+m_{dt})a_1g+k_{dt}a_1^2 & k_{dt}a_1a_2 & k_{dt}a_1 \\ k_{dt}a_1a_2 & -(\frac{1}{2}m_2+m_{dt})a_2g+a_2^2k_{dt} & k_{dt}a_2 \\ k_{dt}a_1 & k_{dt}a_2 & k_{dt}+k_{db} \end{bmatrix} \begin{Bmatrix} \theta_1 \\ \theta_2 \\ u_b \end{Bmatrix} \qquad (1)$$

$$= \begin{Bmatrix} -(\frac{1}{2}m_1+m_2+m_{dt})a_1\ddot{x}_g(t) \\ -(\frac{1}{2}m_2+m_{dt})a_2\ddot{x}_g(t) \\ -(m_1+m_2+m_{db}+m_{dt})\ddot{x}_g(t) \end{Bmatrix}$$

Patterns 21 and 22:

$$\begin{bmatrix} I_{o1}+(m_2+m_{dt})l'^2 & a_1a_2(\frac{1}{2}m_2+m_{dt})-(m_2+m_{dt})\frac{b^2}{2} & m_1a_1+m_{dt}a_1 \\ a_1a_2(\frac{1}{2}m_2+m_{dt})-(m_2+m_{dt})\frac{b^2}{2} & I_{o2}+m_{dt}r_d^2 & \frac{1}{2}m_2a_2+m_{dt}a_2 \\ m_1a_1+m_{dt}a_1 & \frac{1}{2}m_2a_2+m_{dt}a_2 & m_1+m_2+m_{db}+m_{dt} \end{bmatrix} \begin{Bmatrix} \ddot{\theta}_1 \\ \ddot{\theta}_2 \\ \ddot{u}_b \end{Bmatrix}$$

$$+ \begin{bmatrix} -(\frac{1}{2}m_1+m_2+m_{dt})a_1g+a_1^2k_{dt} & k_{dt}a_1a_2 & k_{dt}a_1 \\ k_{dt}a_1a_2 & -(\frac{1}{2}m_2+m_{dt})a_2g+a_2^2k_{dt} & k_{dt}a_2 \\ k_{dt}a_1 & k_{dt}a_2 & k_{dt}+k_{db} \end{bmatrix} \begin{Bmatrix} \theta_1 \\ \theta_2 \\ u_b \end{Bmatrix}$$

$$= \begin{Bmatrix} -(\frac{1}{2}m_1+m_2+m_{dt})a_1\ddot{x}_g(t) \\ -(\frac{1}{2}m_2+m_{dt})a_2\ddot{x}_g(t) \\ -(m_1+m_2+m_{db}+m_{dt})\ddot{x}_g(t) \end{Bmatrix} \qquad (2)$$

where,

k_{db} and k_{dt}	=	effective stiffness of the bottom and top diaphragms respectively;
m_1, m_2	=	effective masses of the lower and upper wall segments respectively;
m_{db} and m_{dt}	=	effective mass of the bottom and top diaphragms respectively;
I_{o1}	=	rotational inertia of the lower wall segment about point O_1 or O'_1;
I_{o2}	=	rotational inertia of the upper wall segment about point O_2 or O'_2;
l'^2	=	$b^2+a_1^2$;
$r_d{}^2$	=	$0.25b^2+a_2^2$; and
$\ddot{x}_g(t)$	=	horizontal acceleration component of ground motion.

3. STIFFNESS MATRIX

The stiffness matrices in Eqs. 1 and 2 are the same and can be re-written in the following form:

$$\mathbf{K} = \mathbf{K_D} + \mathbf{K_G} \qquad (3)$$

where

$$\mathbf{K_D} = \begin{bmatrix} a_1^2k_{dt} & k_{dt}a_1a_2 & k_{dt}a_1 \\ k_{dt}a_1a_2 & a_2^2k_{dt} & k_{dt}a_2 \\ k_{dt}a_1 & k_{dt}a_2 & k_{db}+k_{dt} \end{bmatrix} \qquad (4)$$

and

$$\mathbf{K_G} = \begin{bmatrix} -(\frac{1}{2}m_1+m_2+m_{dt})a_1g & 0 & 0 \\ 0 & -(\frac{1}{2}m_2+m_{dt})a_2g & 0 \\ 0 & 0 & 0 \end{bmatrix} \qquad (5)$$

DOI: 10.1002/eqe

The $\mathbf{K_D}$ component of the stiffness matrix includes the stiffness properties of the timber diaphragms, and $\mathbf{K_G}$ accounts for the negative geometrical stiffness. It will be shown later herein that each of the non-zero elements in $\mathbf{K_G}$ constitutes the bilinear rigid stiffness associated with the restoring effects of the gravitational forces in one wall segment.

3.1. Wall semi-rigid behaviour

Research [2, 3, 7] has shown that the real moment-rotation relationship of cracked URM walls is different to the bilinear model due to finite masonry strength. Trilinear behavioural data has instead been suggested [3, 15], with Fig. 2 detailing a proposed model [15] that is used in this research.

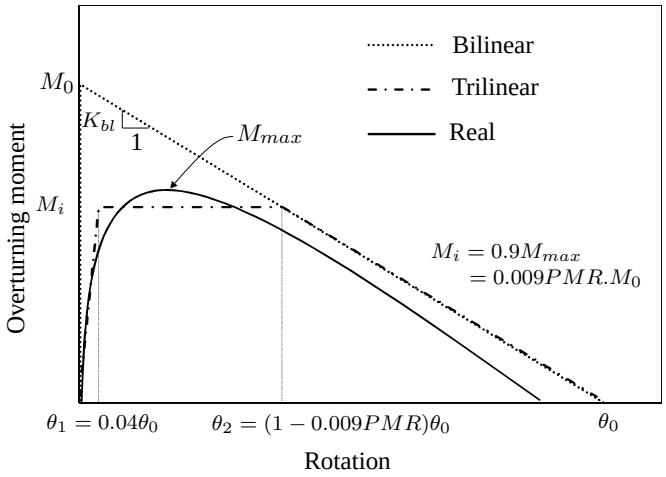

Figure 2. Wall out-of-plane post-cracking behaviour

To construct a trilinear model, the Percentage of Maximum Rigid Resistance (PMR), defined as the ratio of the maximum lateral strength achievable by a real URM wall, M_{max}, to the bilinear rigid strength, M_0, is calculated. This ratio is always less than unity due to the finite masonry compressive strength, which reduces the lever arm of the restoring forces as the wall is subject to out-of-plane rotation [3, 15]. The restoring forces comprise the weight of the wall and the applied overburden, and a reduction in restoring moment results in a reduced wall rotational stiffness. Although refined formula are available in [15], $PMR = 75\%$ could be considered as a conservative lower bound for clay brick URM walls located in single-storey or two-storey buildings. The bilinear data, M_0, and the instability displacement, θ_0, are calculated by studying the free-body diagram of the wall segments as detailed in Fig. 3 and Table I. Other trilinear defining parameters, M_i, θ_1, and θ_2 are next calculated as detailed in Fig. 3, with the 0.009 coefficient being associated with an integer value of 75 for PMR.

Fig. 3 shows a generic URM wall segment and its displaced shape for three cases of applied overburden, sufficient to represent both the upper and lower wall segments in Fig. 1. Considering the equilibrium of the free bodies in Fig. 3, one can obtain the rigid bilinear moment-rotation relationships by equating the overturning and the restoring moments about the rotation pivot at the wall segment base. In conducting these calculations, the moment arms denoted by d_1 to d_4 have algebraic values and can be negative, zero, or positive, depending on the magnitude of θ. The maximum wall moment resistance and instability rotation can next be calculated by substituting, respectively, the lateral displacement and the applied moment with zero. Table I summarises the bilinear parameters for each case, and the following definition has been used in Table I:

$$\psi = \frac{O}{W} \tag{6}$$

where O and W are generic terms and represent the applied overburden and the weight of the wall segment under study.

DOI: 10.1002/eqe

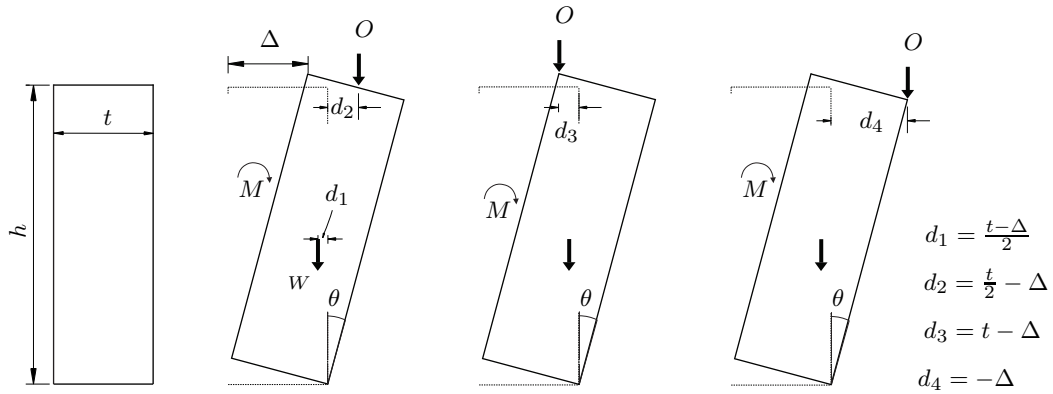

(a) Wall segment (b) Case 1 (c) Case 2 (d) Case 3

Figure 3. Displaced shape of wall segment

Table I. Generic and individual segment bilinear data

(1) Wall segment	(2)	(3) Maximum moment M_0	(4) Instability rotation θ_0	(5) Negative stiffness $K_{bl} = -\frac{M_0}{\theta_0}$
Case 1 (Upper)	Generic	$\frac{tW}{2}(1+\psi)$	$\frac{t}{2h}\frac{1+\psi}{0.5+\psi}$	$-Wh(0.5+\psi)$
	Specific	$(\frac{1}{2}m_2+\frac{1}{2}m_{dt})bg$	$\frac{b}{2a_2}\frac{m_2+m_{dt}}{0.5m_2+m_{dt}}$	$-(\frac{1}{2}m_2+m_{dt})a_2g$
Case 2 (Lower)	Generic	$\frac{tW}{2}(1+2\psi)$	$\frac{t}{h}$	$-Wh(0.5+\psi)$
	Specific	$(\frac{1}{2}m_1+m_2+m_{dt})bg$	$\frac{b}{a_1}$	$-(\frac{1}{2}m_1+m_2+m_{dt})a_1g$
Case 3 (Lower)	Generic	$\frac{tW}{2}$	$\frac{t}{2h}\frac{1}{0.5+\psi}$	$-Wh(0.5+\psi)$
	Specific	$\frac{1}{2}m_1bg$	$\frac{b}{2a_1}\frac{m_1}{0.5m_1+m_2+m_{dt}}$	$-(\frac{1}{2}m_1+m_2+m_{dt})a_1g$

The stiffness properties listed in the last column of Table I are identical to the non-zero diagonals in $\mathbf{K_G}$ (Eq. 5). By using the trilinear representation shown in Fig. 2, one can account for semi-rigid behaviour in the wall response calculations. The equations of motion (Eqs. 1 and 2) will therefore have the stiffness matrix $\mathbf{K_G}$ in the form of a split function representing the trilinear behaviour detailed in Fig. 2. In this study, a MATLAB code was prepared to integrate the nonlinear equations.

3.2. Rotation capacity

It can be found from the expressions in column 4 of Table I that the instability rotation is always less for Case 3 than that for Case 2, where Case 2 represents the lower wall segment in either of Patterns 11 or 12 (Figs. 1b and 1c) and case 3 represents the lower wall segment in either of Patterns 21 or 22 (Figs. 1d and 1e). Combinations of wall thicknesses between 110 mm and 350 mm, wall heights between 3000 mm and 5000 mm, and a top diaphragm seismic weight between 0.75 kPa and 2.10 kPa were considered in a parametric study, and the range of the ratio of the instability rotation (Case 3 to Case 2) was found to be between approximately 0.10 and 0.45. These low ratios signify that in a wall connected to a flexible diaphragm, triggering of Patterns 11 or 12 may result in wall collapse for comparatively low levels of lateral acceleration.

DOI: 10.1002/eqe

3.3. *Wall and diaphragm effective mass and stiffness properties*

As mentioned previously wall mass, diaphragm mass, and the in-plane stiffness of the diaphragms shown in Fig. 1a are effective quantities that must be calculated using principles of structural dynamics. Assuming that each flexible diaphragm is spanning between relatively rigid in-plane loaded masonry walls and that its response is shear-dominated [18] and considering the first mode of deformation, each diaphragm can be represented by a generalised SDOF system [19] and their effective masses, m_{db} and m_{dt}, calculated. Similarly, the wall effective mass, m_1 or m_2, can be calculated with approximations considering that the wall deformation follows that of the timber diaphragm. It is noted that this procedure ignores the two-way effects of the wall and results in overestimation of the wall effective mass. This simplification is however justified given the complex nature of the response and the absense of more accurate study. Calculations [15] have shown that:

$$m_i = \frac{8}{15} m_{nominal,i} \tag{7}$$

where index i is either 1,2, b, or d in Eqs. 1 and 2 and index "nominal" refers to actual mass of the respective structural element. For two out-of-plane loaded walls each connected to opposite ends of a flexible timber diaphragm, the nominal wall mass is equal to the combined mass of the two out-of-plane loaded walls.

The diaphragm stiffness corresponds to the first mode of the in-plane deformation and can be calculated using procedures such as that given in [20, 21], and to obtain the effective geometrical stiffness of the wall, $\mathbf{K_G}$, the wall mass in Eq. 5 is replaced by its effective mass from Eq. 7.

4. INTEGRATION OF THE WALL RESPONSE

The wall rocking pattern may change from one to another during the earthquake excitations, and the wall response includes impact between the wall segments or between a wall segment and the ground. The wall response between any two impacts is governed by a particular equation of motion (Eqs. 1 and 2) and can be integrated separately. At each instance of impact the rocking pattern for the subsequent interval and the appropriate initial conditions should be re-evaluated by investigating the kinematics of impact.

Previous studies [22, 23] proposed similar procedures suitable for free-standing rigid 2-block assemblies subject to ground motion, where at the beginning of the wall response the threshold overturning moments, i.e. M_0 in Fig. 2, are calculated separately for each block and compared with the applied moment. The initial rocking pattern is next determined by comparing the ratio of the applied moment to the threshold moment for all the blocks. Following each impact, the conservation of momentum is used to determine the coefficient of restitution (COR), and this coefficient is in turn used to calculate the initial conditions following the impact and the corresponding rocking pattern. These studies suggested that eight rocking patterns were present, four of them being similar to those shown in Fig. 1. The other four rocking patterns involved the rocking of the top block only or the rocking of the two blocks with the same angle of rotation.

The inclusion of the trilinear (semi-rigid) wall behavioural model (Fig. 2) in the current study implies that the wall segments undergo rocking with the slightest lateral acceleration and therefore there is no threshold moment that must be satisfied. The exclusion of the threshold overturning moment has reduced the rocking patterns to those shown in Fig. 1. The use of the conservation of angular momentum to calculate the coefficient of restitution in the current study is fraught with difficulty due to multiple reasons. One problem is that the principle is only valid when the bodies are in fact rigid and the impact between them is instantanuous. The finite strength and non-rigid nature of the masonry walls have been described by the use of trilinear wall behavioural models in this research, with the models conveying the meaning that the impact between the wall segments cannot be assumed as instantanuous. The other problem is that, unlike the previous studies [22, 23], the wall segments in this research are connected to a flexible diaphragm, which complicates the calculation of the angular momentum before and after the impact. It was considered appropriate for

DOI: 10.1002/eqe

the purpose of this research to calibrate the appropriate COR value range based on available shake table test data.

An event-based time integration procedure was developed using MATLAB software (ODE45 suite), and the method includes detection of the instances of impact (events in ODE45), calculating initial conditions using an assumed COR value, and identifying the appropriate rocking pattern following the flowchart shown in Fig. 4. Multiple solutions are obtained with the only difference between them being the used COR value, and the calculated maximum wall displacement response that best matches the experimental equivalent is presented.

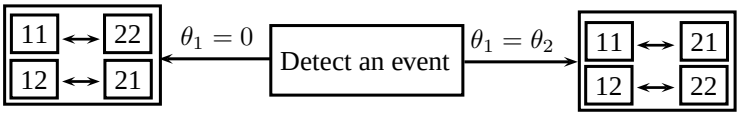

Figure 4. Change in the rocking pattern at the defined events; two-sided arrows indicate that the changes occur in both directions

4.1. Damping

The main sources of energy dissipation during the out-of-plane URM wall rocking response are widely accepted to be the impact between the rocking wall segments in addition to the masonry crushing and elastic and plastic deformations within the wall. Researchers have used various methods to include energy dissipation in the calculation of wall response. A conventional approach based on employing an equivalent viscous damping ratio has been suggested in [3, 4], and a special numerical procedure was employed [3, 11] for single-degree-of-freedom (SDOF) systems. An alternative method based on the use of a coefficient of restitution (COR) has also been used [5, 22, 23] and it has been noted that this method best describes the sudden energy dissipation during each impact.

Additional damping sources should be considered in the numerical modelling when the system under study includes other elements, e.g. flexible diaphragms. As part of the verification study reported herein, shake table test data [9] that included flexible diaphragms that were represented in the tests as elastic springs have been used. The experimental study [9] reported that a viscous damping ratio of either 8% or 12%, depending on the tests, was appropriate to model the energy dissipation through diaphragm deformation. A viscous damping ratio of 12% was therefore used in addition to a constant COR (by calibration) in the verification studies reported herein that included a flexible diaphragm.

5. VALIDATION OF THE MODEL

Experimental results from various shake table single-storey URM wall tests (Table II) conducted by other researchers [3, 10, 24] have been used to validate the numerical model.

Table II. Details of walls used for model verification

Wall* Name	Thickness, b (mm)	Length, l (mm)	Height, h (mm)	Crack height $\frac{a_1}{h}$ —	Wall mass m (kg)	Dia. stiffness k_{db} (N/m)	Dia. stiffness k_{dt} (N/m)	Dia. mass m_{db} (kg)	Dia. mass m_{dt} (kg)
Wall 12	110	1000	1500	0.5	297	1×10^{9}**	1×10^{9}**	0	0
West wall	92	987	1934	0.67	429	1×10^{9}**	5.5×10^{5}	0	780
C9	191	1504	2790	0.48	1739	39.4×10^{3}	37×10^{3}	655	663

* "Wall 12" refers to wall number used in [3], "West wall" is from [10], and "C9" is the name of a test conducted on wall "FF-2" in [24].
** Artificially large value of stiffness to represent rigid support

DOI: 10.1002/eqe

5.1. *Wall characteristic data used in the verification study*

Several wall and diaphragm characteristic properties are required as input information in the numerical model that was used to conduct the verification studies, and these properties were approximated using, or obtained directly from, the data presented in [3] and [10]. The right-hand side of Eqs. 1 and 2 and the mass matrices are straightforward to calculate, but the procedure presented in [15] was employed to calculated the trilinear wall behavioural data involved in stiffness matrices. Table III lists a summary of the approximated wall trilinear properties.

Table III. Details of walls used for model verification

Wall	Segment	PMR, (%)	M_0, (kN.m)	θ_0, (rad)	M_i, (kN.m)	θ_1, (rad)	θ_2,
Wall 12	Upper (Case 1)	72	0.080	0.147	0.052	0.006	0.052
	Lower (Case 2)	72*	0.240	0.147	0.157	0.006	0.052
	Lower (Case 3)	72*	0.080	0.049	0.052	0.002	0.017
West wall	Upper (Case 1)	75**	0.416	0.077	0.281	0.003	0.025
	Lower (Case 2)	75**	0.962	0.071	0.649	0.003	0.023
	Lower (Case 3)	75**	0.130	0.010	0.088	0.0001	0.003
C9	Upper (Case 1)	75***	1.473	0.092	0.994	0.004***	0.030
	Lower (Case 2)	75***	3.722	0.144	2.512	0.006***	0.047
	Lower (Case 3)	75***	0.777	0.030	0.524	0.001***	0.010

* from [3] ** from [15]
*** this row presents only one example of several PMR values assumed

5.2. *Verification results*

Fig. 5a shows that the calculated response of Wall 12 generally matched well with the experimental peak values reported in [3] although significant difference is observed in low-amplitude cycles. Using the model in multiple analyses with different values of COR showed that a COR value of 0.78 produced the most accurate results for Wall 12.

Fig. 5b shows that the calculated response of the West wall [10] has a good correlation with the experimentally recorded values. A COR equal to 0.83 was used, and the numerical model predicted the wall instability that occured at about 5.3 sec.

Figs. 5c to 5e compare the calculated and the experimental displacements for wall C9 reported in [9]. The COR value that produced the best correlation was identified as 0.83, and it was concluded from the three verification studies that a COR value of between 0.78 and 0.83 gives realistic results.

6. EFFECTS OF DIAPHRAGM FLEXIBILITY

A parametric study was conducted by assuming several levels of diaphragm in-plane stiffness for single-storey buildings of various heights and for the top-storey of multi-storey buildings. A procedure and the default material properties suggested by [20] were used to calculate the timber diaphragm stiffness. As a case study, the building plan dimensions of 17.4 m by 29.9 m (similar to an analysed building reported in [25]) were assumed and different configurations of the diaphragms were considered that included single straight sheathing construction (D1 and D2 in Table IV), producing lower bound stiffness properties as per [20] guidelines. As detailed in Table IV, three other cases of diaphragm stiffness were also studied, one corresponding to the stiffness in the long direction of a double diagonal sheathing diaphragm with chords (D3). This type of diaphragm construction is associated with the upper bound of default stiffness properties of as-built timber diaphragms suggested by [20]. The fourth case that was considered is the stiffness in the long

DOI: 10.1002/eqe

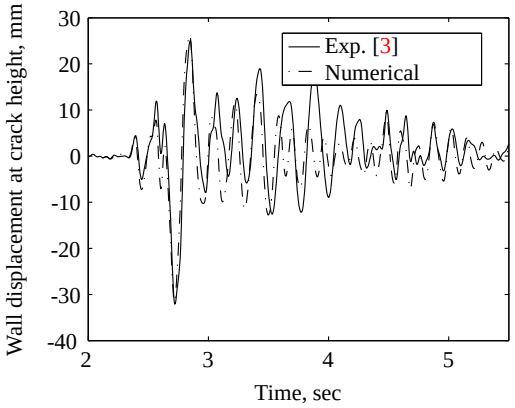

(a) Response of Wall 12, ground motion 400% Nahanni (Nov. 1985)

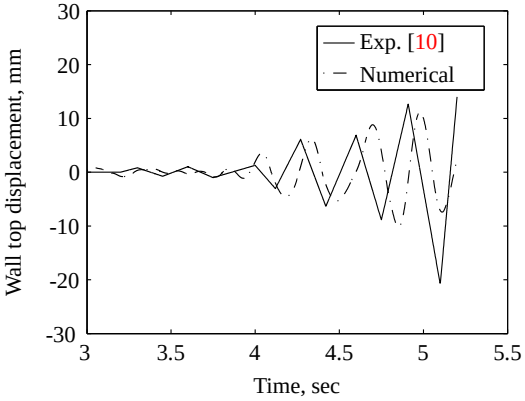

(b) Response of West wall, ground motion 67% Big Bear (June 1992), wall instability at 5.3 sec

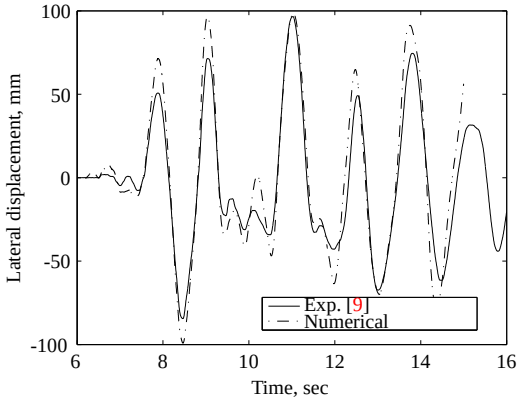

(c) Response at top edge of Wall C9

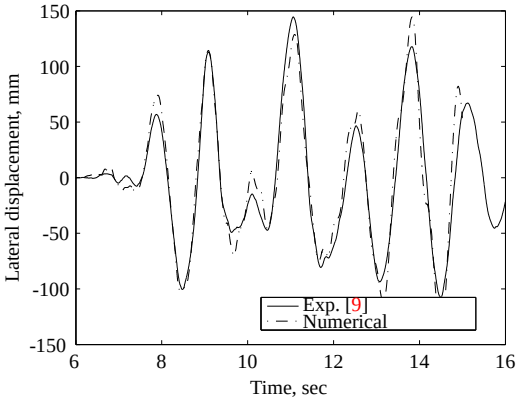

(d) Response of Wall C9 at crack height

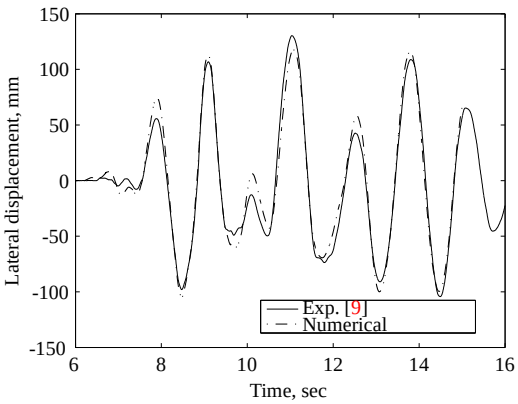

(e) Response at bottom edge of Wall C9

Figure 5. Numerical calculation vs. the experimentally measured response of different walls

direction of a single straight sheathing diaphragm (similar to D2) stiffened using timber overlay (D4) [25]. Finally, a diaphragm with a relatively large in-plane stiffness (D5) was also assumed in the parametric study.

An artificially large stiffness value of k_{db} was assumed for single-storey buildings to account for the ground connection, and for the case of higher-storey walls the top and the bottom diaphragms were assumed to have the same stiffness.

DOI: 10.1002/eqe

Table IV. Diaphragm stiffness for parametric study

	Timber diaphragm description	Direction considered	Calculated stiffness, kN/m	Indicative frequency range*, Hz
D1	As-built with single straight sheathing	short	815 [20]	0.8-1.1
D2	As-built with single straight sheathing	long	2406 [25, 20]	1.4-1.9
D3	As-built with double diagonal sheathing and chords	long	21310[20]	4.2-5.9
D4	Single straight sheathing strengthened with 19 mm plywood overlay with substantial edge nailing	long	40360 [25]	5.9-7.7
D5	Artificially large stiffness value representing pinned top support	—	1×10^6	30-40

* For the purpose of frequency calculations the diaphragm was envisaged as a SDOF system having an effective mass equal to half the mass of the out-of-plane loaded walls plus the effective mass of the diaphragm and having the stiffness listed.

The out-of-plane loaded walls were assumed to be double-wythe (230 mm thick) and of varying height, resulting in slenderness ratios ranging from 8 to 24. A variety of earthquake accelerograms were adopted to include ground motions covering a wide range of frequency content, as detailed in Table V. The wall crack height was assumed to be at two-thirds of the wall height from the wall base, and a COR of 0.8 was assumed consistently in all the analyses.

Table V. Details of earthquake accelerograms used for model verification

Earthquake Name	El Centro	Nahanni aftershock	Christchurch
Location	El Centro	Iverson, Canada	Christchurch, New Zealand
Date	18/05/1940	23/11/1985	22/2/2011
Magnitude	6.6	5.5	6.3
Epicentral Distance, km	8	7.5	10
Station	—	Site1	REHS
Site Geology	Rock	Rock	Deep alluvium
Component	NS	10	N02E
PGA, g	0.35	0.23	0.37
Significant frequency range, Hz	0.2-7.0	7.0-9.0	0.2-3.0
Scale factor	0.5	4.0	0.5

A total of 135 direct time integration analyses (5 timber diaphragm stiffness properties, 9 walls, and 3 earthquake records) were conducted for single-storey walls and 108 analyses were conducted for higher-storey walls (4 timber diaphragm stiffness properties, 9 walls, and 3 earthquake records). A report of the absolute maximum acceleration ($A_{max,abs}$) and displacement ($D_{max,abs}$) response calculated for single-storey walls subject to one of the earthquakes (the 22nd February 2011 Christchurch earthquake) is first presented, followed by a detailed evaluation of the wall rocking pattern and stability for both single-storey and multi-storey buildings. The absolute maximum acceleration values are important in the evaluation of the effect of diaphragm flexibility on the seismic force demand imposed on the wall and on the wall-diaphragm connections. The study of wall rocking pattern is crucial in evaluating wall stability and involves reviewing "snapshots" of the wall displacement profile for the entire displacement history.

DOI: 10.1002/eqe

6.1. *Absolute maximum acceleration response*

The absolute maximum acceleration ($A_{max,abs}$) at the wall top generally increased with increasing diaphragm stiffness, as shown in Fig. 6a. This increase in the imposed accelerations, particularly at the wall top, suggests that timber diaphragm stiffening should probably be accompanied by strengthening of URM walls in the out-of-plane direction and by the retrofit of wall-diaphragm connections.

The acceleration at the crack height also slightly increased with the diaphragm stiffness as shown in Fig. 6b, with the increase from D1 to D4 being nearly 50% for the most dramatic case, associated with the wall having the lowest slenderness ratio (8).

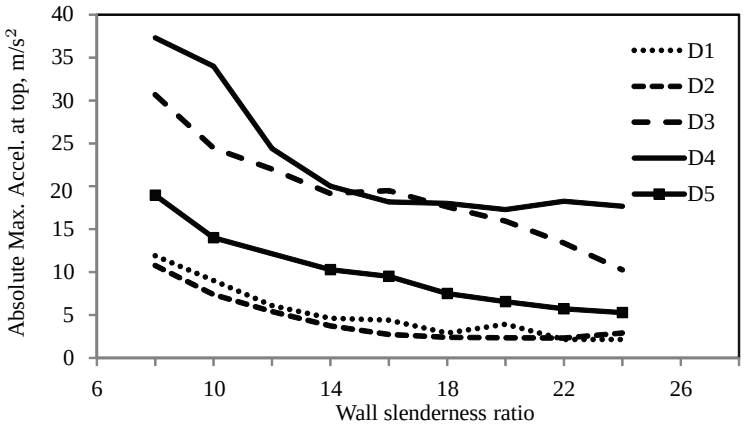

(a) Acceleration response at wall top

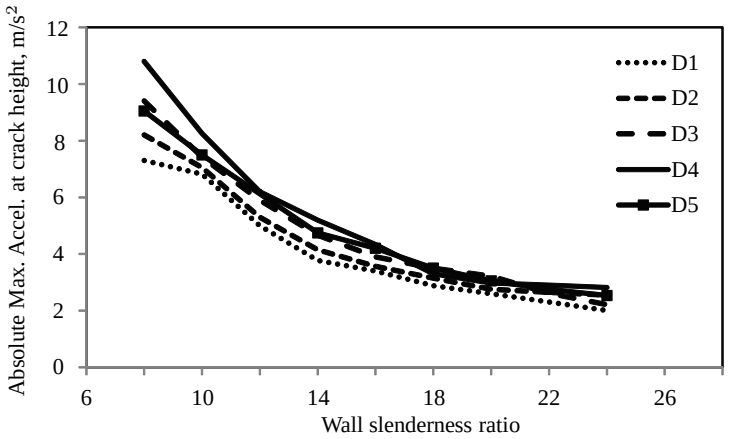

(b) Acceleration response at crack height

Figure 6. The acceleration response of the out-of-plane loaded walls connected to different diaphragms

6.2. *Absolute maximum displacement response*

In contrast to wall acceleration response, the calculated absolute maximum wall displacements ($\Delta_{max,abs}$) at wall top generally reduced with increased stiffness of the top diaphragm. Fig. 7a shows that $\Delta_{max,abs}$ at the wall top remained almost constant for the entire range of the assumed wall slenderness ratios but for most walls decreased with increasing stiffness of the top diaphragm. Fig. 7b shows that the change in $\Delta_{max,abs}$ at the crack height is irregular with respect to the changes in the diaphragm stiffness and/or wall slenderness ratio. The influence on wall stability due to the greater and smaller displacement occuring, respectively, at the crack height and at the wall top is considered in the next section.

DOI: 10.1002/eqe

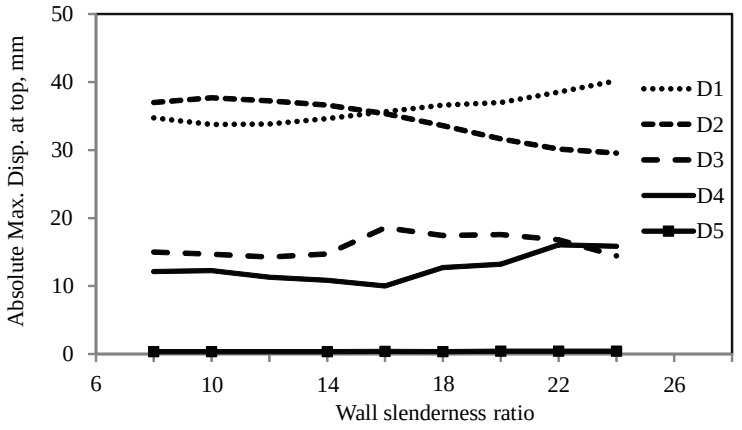

(a) Displacement response at wall top

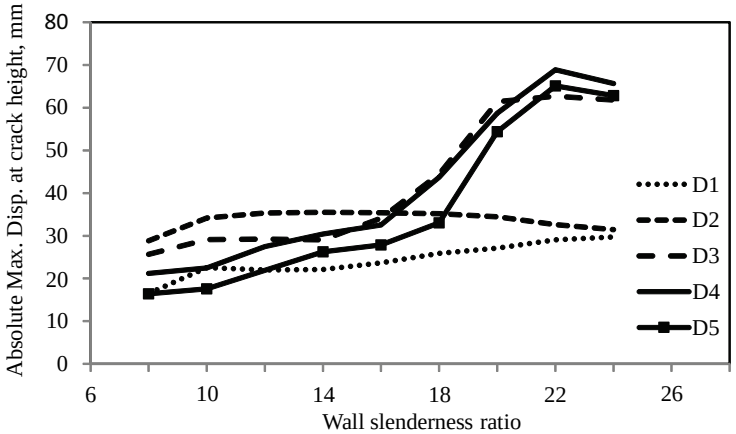

(b) Displacement response at crack height

Figure 7. The displacement response of the out-of-plane loaded walls connected to different diaphragms

6.3. *Wall stability*

6.3.1. Single-storey buildings Fig. 8a and 8b show the calculated displacement response histories for a 4140 mm high wall (slenderness ratio of 18) at the wall top and at the wall crack height, respectively. The evaluation of the stability of this wall is first reported, and the summary of similar studies for other configurations are reported at the end of this section.

As discussed earlier, Patterns 21 and 22 are more favorable than Patterns 11 and 12 due to the increased wall instability displacement for the lower wall segment. An investigation of Fig. 8 showed that the wall connected to the rigid diaphragm (D5) was responding in unfavourable rocking patterns (11 or 12) for only 1.5% of the duration of the excitation. The $\Delta_{max,abs}$ imposed at the top of the lower wall segment (33 mm displacement at crack height) remained within 14% of the instability displacement for this wall segment as detailed in columns 2, 5, and 7 of Table VI. In contrast, the wall with flexible diaphragm (D1) responded in unfavourable patterns for more than 50% of the total duration, and the $\Delta_{max,abs}$ recorded at the crack height and in one of these two patterns was 22 mm. Despite this displacement being smaller than the equivalent for the case of the pinned top support (D5), the wall is deemed less stable due to the reduced wall instability displacement in Patterns 11 and 12. The $\Delta_{max,abs}/\Delta_{ins}$ ratio of the lower wall segment was calculated as 35%, as opposed to 14% for the case of D5.

The top wall segment stability was also investigated as reported in columns 3, 4, and 6 of Table VI. The overall wall stability was judged based on the instability ratio that was greater, as detailed in column 8 of Table VI.

DOI: 10.1002/eqe

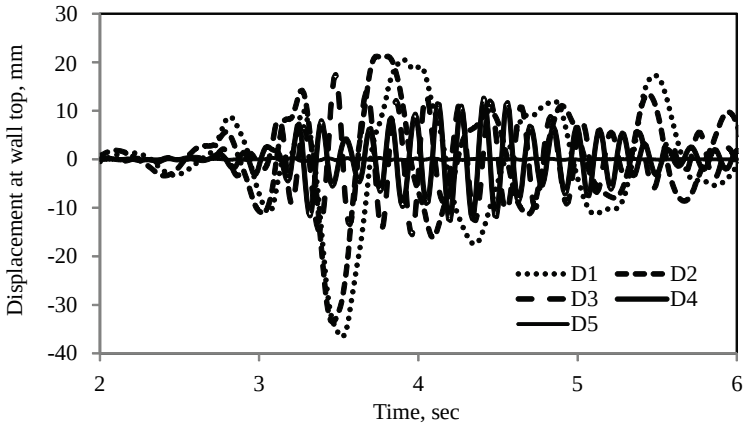

(a) Displacement response history at wall top

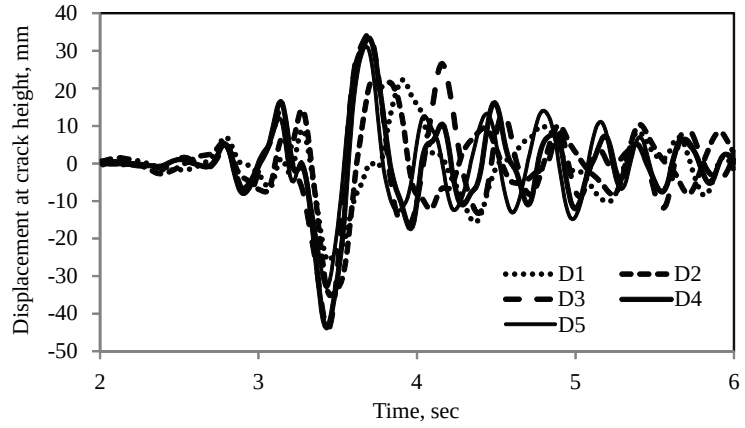

(b) Displacement response history at crack height

Figure 8. Displacement response history for wall with slenderness ratio of 18 (wall height=4140 mm, thickness=230 mm)

Table VI. Investigation of the stability of wall segments

(1)	(2)	(3)	(4)	(5)	(6)	(7)	(8)
	$\Delta_{max,abs}$		Δ_{ins}		Instability ratio ($\Delta_{max}/\Delta_{ins}$)		
Case	crack height	Differential (top-crack height)	upper	lower	upper	lower	max (6&7)
D5	33	47	230	230	0.20	0.14	0.20
D1	22	16	230	62	0.07	0.35	0.35

The above study was repeated for all combinations of walls, diaphragms, and earthquake loadings. Figure 9 shows the governing (greater) instability ratio ($\Delta_{max,abs}/\Delta_{ins}$) of the lower and upper wall segments over a range of slenderness ratios. Figs. 9a to 9c show that for most wall and diaphragm configurations the instability ratio increases, i.e. the wall destabilises, with diaphragm flexibility. There are many situations where the wall stability significantly improves (instability ratio decreases) with diaphragm flexibility. For example, for cases using the Nahanni earthquake ground motion, Fig. 9a, walls with slenderness ratios greater than 18 become more stable when the diaphragm case was changed from D3 to D2.

DOI: 10.1002/eqe

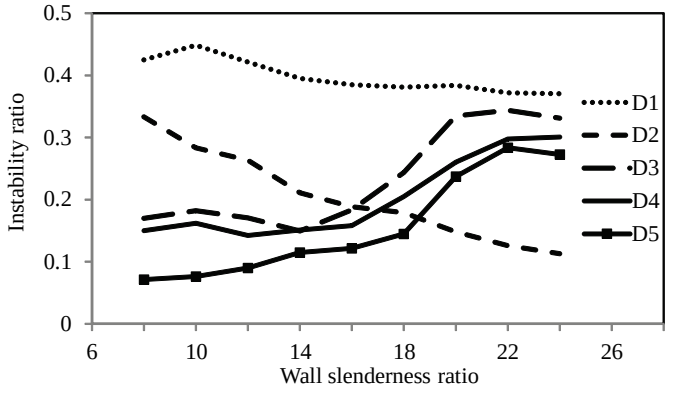

(a) Nahanni earthquake; Double-wythe wall

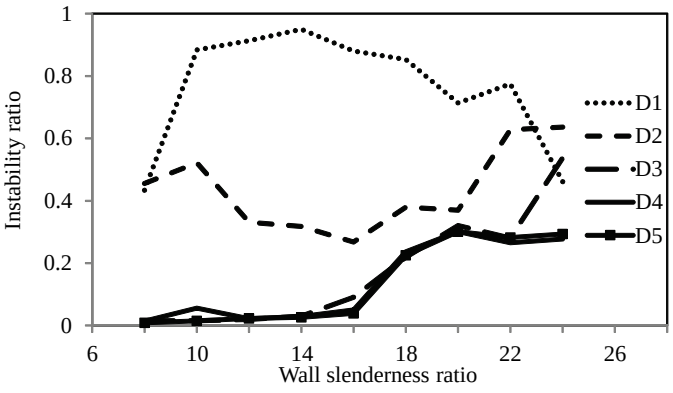

(b) Christchurch earthquake; Double-wythe wall

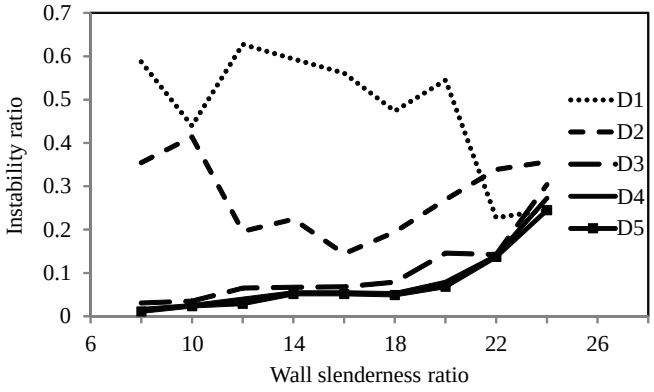

(c) El Centro earthquake

Figure 9. Stability of single-storey walls vs. slenderness ratio

The instability ratio generally increases consistently with wall slenderness ratio when the wall is connected to D3 or stiffer diaphragms. The relationship between the wall slenderness ratio and stability for walls connected to either D1 or D2 is chaotic in Figs. 9b and 9c, and the calculated instability ratio does not correlate with the wall slenderness ratio, which is a criterion that is commonly used to evaluate the stability of out-of-plane loaded URM walls [20]. As the stiffness of the timber diaphragm increases, the instability ratio converges to that for the case of the pinned top support. It may therefore be possible to identify a value of the timber diaphragm stiffness at which walls behave in a simply-supported condition.

DOI: 10.1002/eqe

While the development of seismic assessment methodology for out-of-plane loaded walls is outside the scope of this study, and considering the significant variation in the resulting trends between the 3 ground motions that were used, it is recommended that a more detailed study that includes site-specific ground motion records be conducted and that a suitable seismic assessment procedure is developed.

6.3.2. Higher storey walls Similar to the case of single-storey walls, both stabilising and destabilising effects of the diaphragm flexibility can be observed for higher storey walls. Figure 10a shows that the Nahanni earthquake that was characterised by high frequency shaking caused the walls connected to stiffer diaphragms to become less stable than the walls connected to more flexible diaphragms. Conversely, for the low-frequency 2011 Christchurch earthquake record (Table V), the wall stability reduced with diaphragm flexibility (Figure 10b).

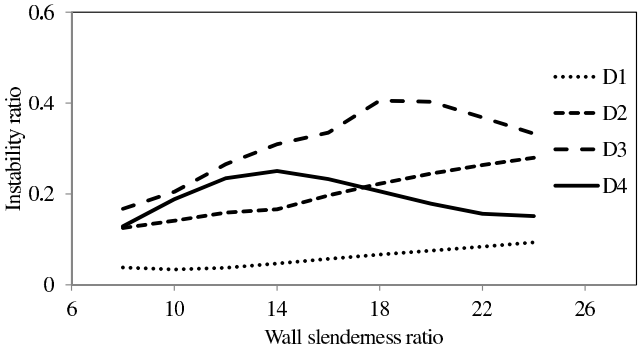

(a) Nahanni earthquake

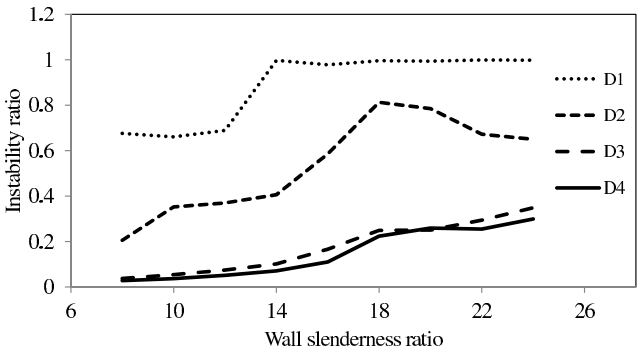

(b) Christchurch earthquake

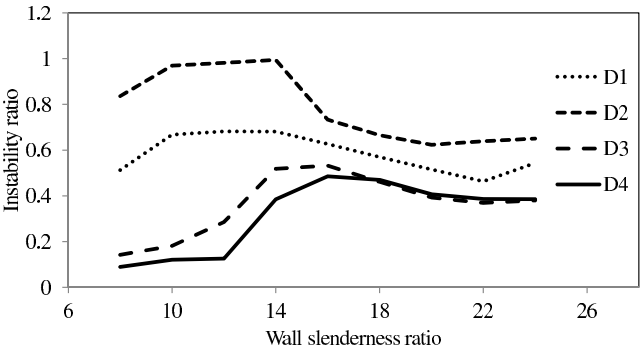

(c) El Centro earthquake

Figure 10. Stability of higher storey walls vs. slenderness ratio

DOI: 10.1002/eqe

For the El Centro earthquake that included a wide range of significant frequencies, there is no clear relationship between the diaphragm flexibility and the wall stability as evident from Figure 10c. Similar to the case of walls connected to one flexible diaphragm, the stability of the walls connected to two flexible diaphragms appears to have no obvious relationship with the wall slenderness ratio for the ground motion records that were considered.

Considering the indicative frequency range calculated for the diaphragms in the analysed buildings (see Table IV), the frequency range of the earthquake records (see Table V), and the above discussion of Figure 10, it appears that walls connected to two flexible diaphragms are worst affected by the earthquakes that have a dominant frequency comparable to that of the diaphragms.

Current seismic assessment codes and guidelines [20, 26] do not differentiate between walls connected to rigid or to flexible diaphragms. Based on the limited parametric study presented herein, it is suggested that a more detailed parametric study that would include a wider range of ground motion records be conducted. The detailed study should be aimed at, first, assessing the suitability of the wall slenderness ratio or an alternative parameter as a criterion for the seismic assessment when timber diaphragms are in as-built conditions. Second, the study should include the development of a procedure that incorporates the resonance effects that occur when an earthquake has similar dominant frequency content to the main frequency of the diaphragms.

7. SUMMARY AND CONCLUSIONS

A simplified numerical model was presented for the analysis of out-of-plane loaded walls in URM buildings with flexible diaphragms. The equations of dynamic motion were obtained using principles of rocking mechanics of rigid bodies and the formulae were next modified to include semi-rigid wall behaviour. The wall rotation capacity was quantified as a function of the wall rocking pattern, and it was found that certain rocking patterns that are triggered due to diaphragm flexibility are associated with a reduced wall rotation capacity.

An event-based numerical procedure was used to integrate the wall response by considering the impact between the rocking wall segments and the ground. A verification study showed that the model predicted wall response reasonably accurately, but that the model often overestimated low-amplitude wall response. The capability of the model to predict wall peak response suggests that it is a reliable tool for the purpose of wall seismic assessment based on instability displacements.

A parametric study was conducted to investigate the effects of diaphragm flexibility on the response of out-of-plane loaded walls located in single-storey or multi-storey buildings. Results showed that out-of-plane loaded walls are subject to greater earthquake accelerations, particularly at the location of the wall-diaphragm connections when common timber diaphragm stiffening practices are employed. It is suggested based on this investigation that if diaphragm stiffening is undertaken in a URM building, then this work should be accompanied by the retrofit of out-of-plane loaded wall-diaphragm connections and by the retrofit of out-of-plane loaded walls.

The study suggests that the effect of diaphragm flexibility on wall stability is dependent on the applied ground motion. It was found that higher storey walls connected to two horizontal diaphragms had reduced stability for applied earthquake accelerograms having dominant frequency content that was comparable to the frequency of the diaphragms. It was also found that the URM wall stability did not correlate well with the wall slenderness ratio for the ground motion records that were used, and further study was recommended based on these findings.

ACKNOWLEDGEMENTS

The authors greatly acknowledge the financial support provided by the Australian Research Council (ARC). The authors also wish to acknowledge the financial support provided by the New Zealand Government via the Foundation for Research, Science, and Technology (FRST). The authors wish to acknowledge Dr. Osmar Penner for the shake table test data and comments on the study.

DOI: 10.1002/eqe

REFERENCES

1. ABK. Methodology for mitigation of seismic hazards in existing unreinforced masonry buildings: Wall testing, out-of plane. *Technical Report ABK-TR-04*, ABK, A Joint Venture 1981.
2. Priestley MJN. Seismic behaviour of unreinforced masonry walls. *Bulletin of the New Zealand Society for Earthquake Engineering* 1985; **18**(2):191–205.
3. Doherty KT. An investigation of the weak links in the seismic load path of unreinforced masonry buildings. PhD thesis, Faculty of Engineering of The University of Adelaide 2000.
4. Griffith MC, Magenes G, Melis G, Picchi L. Evaluation of out-of-plane stability of unreinforced masonry walls subjected to seismic excitation. *Journal of Earthquake Engineering* 2003; **7**(1):141–169.
5. Sorrentino L, Masiani R, Griffith MC. The vertical spanning strip wall as a coupled rocking rigid body assembly. *Struc Eng Mech* 2008; **29**(4):433–453.
6. Sharif I, Meisl CS, Elwood KJ. Assessment of ASCE 41 height-to-thickness ratio limits for URM walls. *Earthquake Spectra* 2007; **23**(4):893–908.
7. Derakhshan H. Seismic assessment of out-of-plane loaded unreinforced masonry walls. PhD thesis, The University of Auckland, New Zealand 2011.
8. Priestley M, Calvi G, Kowalsky M. *Displacement-Based Seismic Design of Structures*. IUSS Press: Pavia, Italy, 2007.
9. Penner O. Effect of diaphragm flexibility on out-of-plane dynamic stability of unreinforced masonry walls. PhD thesis, The University of British Columbia 2014.
10. Simsir CC. Influence of diaphragm flexibility on the out-of-plane dynamic response of unreinforced masonry walls. PhD thesis, University of Illinois at Urbana-Champaign 2004.
11. Lam NTK, Griffith M, Wilson J, Doherty K. Time-history analysis of URM walls in out-of-plane flexure. *Engineering Structures* 2003; **25**(6):743–754.
12. Menon A, Magenes G. *Out-of-Plane Seismic Response of Unreinforced Masonry - Definition of Seismic Input*. IUSS Press, ROSE School: Italy, 2008.
13. Costley AC. Dynamic response of URM buildings with flexible diaphragms. PhD thesis, University of Illinois at Urbana-Champaign 1995.
14. Tena-Colunga A. Seismic evaluation of unreinforced masonry structures with flexible diaphragms. *Earthquake Spectra* 1992; **8**(2):305–318.
15. Derakhshan H, Griffith M, Ingham J. Out-of-plane behaviour of one-way unreinforced masonry walls. *ASCE Journal of Engineering Mechanics* 2013; **139**(4):409–417.
16. Derakhshan H, Griffith M, Ingham J. Airbag testing of multi-leaf unreinforced masonry walls subjected to one-way bending. *Engineering Structures, available online http://dx.doi.org/10.1016/j.engstruct.2013.10.006* 2013; **57**(1):512522.
17. Derakhshan H, Griffith M, Ingham J. In-situ out-of-plane testing of as-built and retrofitted unreinforced masonry walls. *ASCE Journal of Structural Engineering, available online 10.1061/(ASCE)ST.1943-541X.0000960* 2014; .
18. Wilson A, Quenneville P, Ingham J. Natural period and seismic idealization of flexible timber diaphragms. *Earthquake Spectra* 2013; **29**(3):1003–1019.
19. Clough R, Penzien J. *Dynamics of Structures, 3rd Edition*. Computers & Structures, Inc.: Berkeley, USA, 2003.
20. ASCE. *Seismic Rehabilitation of Existing Buildings, ASCE/SEI 41-06*. American Society of Civil Engineers: Reston, VA, 2007.
21. Giongo I, Wilson A, Dizhur D, Derakhshan H, Tomasi R, Griffith M, Quenneville P, Ingham J. Detailed seismic assessment and improvement procedure for vintage flexible timber diaphragms. *Bulletin of the New Zealand Society for Earthquake Engineering* 2014; **47**(2):97–118.
22. Psycharis IN. Dynamic behaviour of rocking two-block assemblies. *Earthquake Engineering and Structural Dynamics* 1990; **19**(4):555–575.
23. Spanos P, Roussis P, Politis N. Dynamic analysis of stacked rigid blocks. *Soil Dynamics and Earthquake Engineering* 2001; **21**(7):559–578.
24. Penner O, Elwood K. Shake table study on out-of-plane dynamic stability of unreinforced masonry walls. *12th Canadian Masonry Symposium*, Vancouver, BC, Canada, June 02-05, 2013.
25. Oliver S. A design methodology for the assessment and retrofit of flexible diaphragms in unreinforced masonry buildings. *SESOC Journal, New Zealand* 2010; **23**(1):19–49.
26. NZSEE. *New Zealand Society for Earthquake Engineering (NZSEE): Assessment and Improvement of the Structural Performance of Buildings in Earthquakes*. Recommendations of a NZSEE Study Group on Earthquake Risk Buildings, 2006.

DOI: 10.1002/eqe